Physics – Uspekhi **50** (5) 513 – 528 (2007)

REVIEWS OF TOPICAL PROBLEMS PACS numbers: **07.60.–j**, **87.16.–b**, **87.64.–t**

Dynamic phase microscopy: is a 'dialogue' with the cell possible?

V P Tychinskii

DOI: 10.1070/PU2007v050n05ABEH006222

Contents

Abstract. The metabolic component of refractivity is considered as an example of a quantifying parameter for the 'vitality' of cells and organelles. It is shown that intracellular processes can be studied by the dynamic phase microscopy method, which provides real-time information in the form of local changes in the optical path difference. Preliminary results demonstrate the possibility of localizing a 'signal' and obtaining information under the signal – structure – function scheme and show prospects for conducting a 'dialogue' with a cell by real-time registering the way in which it responds to changes in external conditions. The mechanism underlying the dependence of refractivity on metabolic states is explained by the contribution of bound water molecules.

1. Introduction

It is known from the history of natural sciences that the perception of natural phenomena is especially productive when a 'dialogue' with the object of interest is possible. The dialogue with the cell in the form of registration of its response to external factors dates from the time when optical microscopy made it possible to correlate morphological structure with function. In the course of further studies, cells and microorganisms were found to undergo metabolism-dependent fluctuations of various parameters (both physical and biochemical) with frequencies ranging from hundredths to hundreds of Herz [1]. New microscopic techniques [2] gave impetus to more systematic studies of individual cell and organelle responses. Mitochondria proved to be a unique biological object whose physiological state can be described by a physically measurable parameter [3]. Specifically, the use of fluorescent labels built in a mitochondrial membrane permitted recording time-dependent changes of membrane potential induced by a variety of substrates added to the incubation medium [4, 5]. These [4, 5] and other [6] works demonstrated that 'voices' of individual organelles contain much more information than the 'polyphonic chorus' of their population. Therefore, new physical methods allowing a deeper insight into the mysterious world of intracellular phenomena became an important supplement to the traditional biological techniques emerging from what is known in the literature as the 'structure – function' concept [7]. Formulated in simple terms, it provides a tool for the study of structure – function relationships. Biological structures are usually described by features visible in cell and organelle images and their functions by quantitative parameters of biochemical processes averaged over large populations. This approach ignores the nonstationary character of intracellular 'events,' cooperative processes, their spatio-temporal correlations, etc.

For a variety of well-known reasons, traditional physical methods proved virtually unsuitable for the description of processes in biological objects. One of the obstacles is the lack of sufficiently universal, physically determined quantitative parameters describing an object and the invasive character of the existing measuring techniques. Moreover, the mechanism of the dependence of the physical parameter being measured on the functional state of the object is in many cases unknown (mitochondria being an exception).

To designate these manifold problems, it is proposed to supplement the structure – function concept by an arbitrary term 'signal' and use the word combination 'signal – structure – function' (SSF). In this new concept, the purpose of the dialogue is formulated as the establishment of the cause-and-effect relationship between processes in morphologically determined structures (organelles), their biochemical and physiological functions, on the one hand, and adequate real-

V P Tychinskii Moscow State Institute of Radio Engineering, Electronics and Automation (Technical University)
Prosp. Vernadskogo 78, 119454 Moscow, Russian Federation
Tel. (7-495) 434 67 92. Fax (7-495) 434 86 65
E-mail: vtych@yandex.ru

Received 1 February 2007
Uspekhi Fizicheskikh Nauk **177** (5) 535 – 552 (2007)
Translated by Yu V Morozov; edited by A M Semikhatov

time 'signals' containing information (a response) sufficient for the decision-making, on the other hand. A hypothetical example of such a response is a decrease in the refractivity fluctuation amplitude associated with a slowdown of pre-ribosome synthesis induced by lowering the cell temperature.

We briefly indicate a list of problems related to the SSF concept. Requirements for the method and measuring device, availability of test objects, unification of methods, etc. deserve special consideration. A large amount of work is needed to classify and interpret signals, distinguish their universally significant parameters; a 'Rosetta stone' will be needed to translate signals of different origins into the biophysical language. Resolution of these problems is a challenge for physicists and biophysicists. The aim of this paper is to draw attention to the interdisciplinary problem conventionally called dialogue and to illustrate the possibility, in principle, of its solution.

The list of basic issues that are promising in terms of realization of the dialogue problem include

— cooperativity of transcription and protein synthesis processes;

— the relationship between gene expression and transcription, and protein synthesis and transport; temporal characteristics of these processes;

— investigation into factors influencing cell adaptation to variations in the external milieu;

— interactive gene engineering, control of transcription processes.

Solving these and related problems is possible if a variety of methods are employed, including new ones that ensure access to spatio-temporal information at the level of individual cells and organelles. However, the potential of modern optical, electronic, and computational technologies is far from being exhausted in the development of noninvasive methods for insight into intracellular dynamics.

There are several reasons for which a dialogue with the cell still lacks the desired efficiency:

(1) The enormous complexity of the system in question, its variation in time, the lack of physical models, the interdependence of processes, and an indefinite number of parameters.

(2) A deficit of fundamental knowledge about the mechanisms of the dependence of physical parameters of a given object on its functional state and metabolic processes.

(3) A lack of noninvasive methods and quantitative data about and functional characteristics of the objects of interest.

(4) The limited sensitivity and poor spatio-temporal resolution of the available methods.

In this work, we attempt to answer the following questions:

— What physical parameters of the cell that are measurable in real time contain functionally significant information? What conditions are necessary to register signals?

— What new fundamental knowledge of cell biology can be expected from the real-time dialogue with an individual cell or a microorganism?

— What is the predicted value of the expected results for the solution of topical problems in biology, ecology, and medicine?

2. Overview of optical methods for investigations into intracellular dynamics

This section is confined to optical microscopic techniques, because electron microscopy is unfit to study processes in living cells and scanning probe/atomic force microscopy is not yet widely applied. As mentioned above, quantitative data about the dependence of the membrane potential on the functional state of mitochondria have been obtained by fluorescent microscopy [4 – 6]. The procedures of fluorescent labeling (e.g., using TMRE), gauging the membrane potential (MP), and artifact evaluation have been discussed at length in [4, 5]. MP fluctuations in mitochondria appear to spread over the entire membrane, although data on their spatio-temporal correlation have not been given. An advantage of the method is the possibility of spectral analysis of fluorescent signals. The main drawbacks of fluorescent microscopy have been extensively discussed in the literature. Here, they are formulated as the following theses:

(1) Labeling affects the object state; hence, the necessity to thoroughly control dye concentration. Active forms of oxygen arise from dye dissociation.

(2) MP gauging is unrelated to physical standards; it is expressed in arbitrary units and depends on many factors, such as the source spectrum and intensity, sensitivity, and spectral characteristics of the photodetector.

(3) Illumination intensity and sensitivity of the camera restrict the exposure time and operating speed to several seconds.

(4) Spatial resolution in studies of local dynamic processes is insufficient despite recent achievements in fluorescent microscopy, e.g., the detection of submicron structures, small clusters in nucleoli, and even isolated macromolecules.

CARS and different variants of combination nonlinear spectroscopy [8 – 10] are worth mentioning among methods whose potential for studying intracellular dynamics is not yet realized in full measure. Their important advantages include the possibility of registering vibrational frequencies of macromolecules [9, 10] associated with metabolically induced structural changes.

For a variety of reasons (see below), the interference techniques and their relatively recent modifications are more promising for intracellular dynamics studies [11 – 23]. Of primary importance for functional state diagnosis is the relationship between the optical path difference (OPD) measured by the interference method and the refractive index, a macroscopic parameter of the medium [11, 19, 20, 23]. Many factors directly or indirectly indicate that phase thickness (or OPD) depends on the object functional state [11, 13-17, 19, 20, 23 – 30]. The prospects for applying coherent interferometry to the study of intracellular dynamics seem to have been first demonstrated in [11]. Only a few recent reports are mentioned below to avoid a comprehensive review of the large number of studies published after [11]. They concern the measurement of refractivity in chloroplasts [24], cyanobacteria [25], spores [25], and cells [26 – 30], which confirmed the diagnostic value of the refractive index of various biological objects. The changes in refractivity under hypotonic stress observed in measuring neurons by holographic microscopy were considered paradoxical in [19]. The authors of [19] explain impaired refractivity under hypotonic conditions by lowered protein concentration (rather than altered functional state — *V.T.*). Hilbert phase microscopy [20] revealed reduced phase thickness following erythrocyte hemolysis that resulted in a 50% decrease in their volume for 4 seconds. The possibility of using refractometry in flow-through cuvettes by Hilbert microscopy for diagnostic purposes was demonstrated in [23]. These observations agree with earlier findings [24 – 26].

An adequate model of a biological object is of primary significance for the application of interference methods, diagnostics, and interpretation of the obtained results. An optically inhomogeneous real object is usually presented as a uniform sphere with an equivalent refractive index. In a few cases, the phase image can be separated into constituent structural elements to measure their refractivity. Both geometric thickness and refractivity contribute to OPD; hence, the importance of their separation and the accuracy of refractive index measurement for the discovery of minor changes in the functional state.

Two immersion media with known refractive indices were used in [19] to distinguish between contributions of physical thickness and refractive index to OPD. However, a more promising approach [23] appears to be the use of a cell from a material with a known refractive index because it markedly simplifies measurements and improves their accuracy. Hilbert phase microscopy with a common optical path [23] ensured high accuracy of measurements, low sensitivity to vibrations, and millisecond time resolution. Spatial resolution in this method was limited by diffraction on the objective aperture.

The potential of coherent phase microscopy (CPM) and its modifications [11, 12, 23 – 30] is considered at length in the next section. Here are the main inferences.

The use of interference methods in intracellular dynamics studies has a number of advantages over other optical methods. These high-performance methods are less invasive (e.g., they do not require fluorescent markers) and more sensitive, and permit representing the local optical path difference (or phase thickness) as values normalized to the wavelength. Unstained cells are optically inhomogeneous structures producing a rather high contrast in an interference microscope. Their organelles are easy to distinguish by optical density. Results reported in [11 – 30] confirm the possibility of obtaining new information about intracellular metabolic processes. However, the use of both traditional and certain novel optical techniques [19 – 23] is substantially restricted by their low spatial resolving power limited by diffraction on the objective aperture. The size of organelles is typically smaller than or comparable to the wavelength. The possibility of substantial spatial superresolution in phase images was first demonstrated in [32 – 34].

3. Airyscan coherent phase microscope, dynamic phase microscopy

The results of measurements presented below and published in [11, 12, 24 – 34] were obtained with an Airyscan coherent phase microscope (CPM) created at the Moscow State Institute of Radio Engineering, Electronics and Automation (MIREA) [11, 12]. Its optical scheme is shown in Fig. 1. The microscope is a modified Linnik interferometer with a helium – neon laser as a source of coherent radiation. Registration of an interference signal and its analog-to-digital conversion to local phase values were performed by means of a periodic modulation of the reference wave phase with the use of a coordinate-sensitive photodetector (dissector and electronic unit). The main difference from other interference methods for generating phase images (e.g., those described in [13 – 23]) was the successive OPD measurement at each point of the image. The sampling periodicity and the image loading rate were determined by the modulation frequency (1 kHz or 1 ms per pixel). The operating speed was limited by the modulation frequency, but the resulting phase images had a number of important advantages. Specifically, they differed from images obtained by traditional [13 – 17], multistep [18], and Hilbert [20 – 23] microscopy by a higher spatial resolution (up to 100 nm in static [11, 12, 33, 34] and 25 nm in dynamic [32] phase images); also, random access to individual points of the image was feasible. The working field of the microscope could be varied in the 5 – 50 μm range depending on the study object; the maximum dimension along a single coordinate was as large as 1024 pixels. The noise-limited sensitivity was $h_{\min} = 0.5$ nm. The phenomenon of superresolution observed in phase images [32 – 34] by CPM pertains to basic optical problems and is not discussed here. Suffice it to mention that limitation of the spatial resolution by the Rayleigh criterion does not extend to functional images, including certain phase ones.

A CPM software packet was used to obtain topograms and 3D-phase images of objects and their fragments, to edit files, to

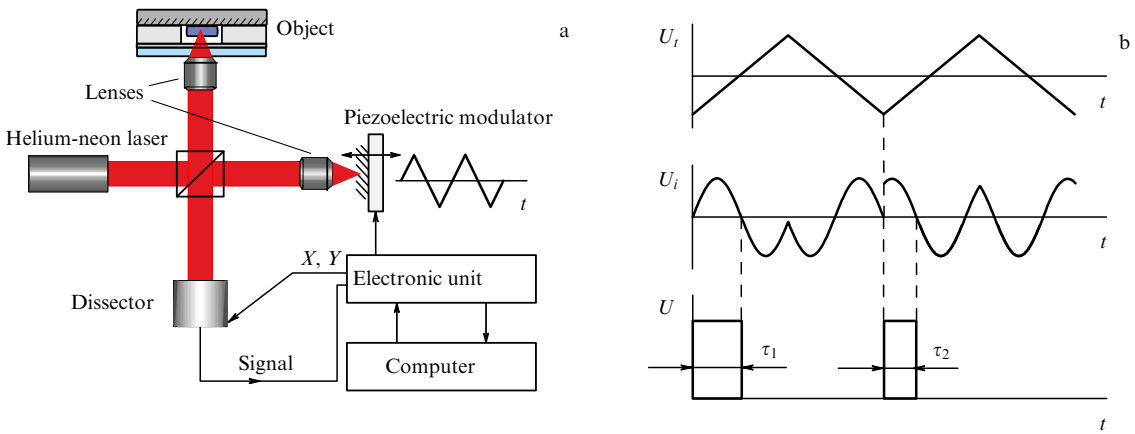

Figure 1. Coherent phase microscopy. (a) The optical scheme of the Airyscan coherent phase microscope includes a source of coherent radiation (laser $\lambda = 633$ nm) and linear-periodic modulation of the reference wave phase. The phase in each pixel of the interference image was determined by means of its successive scanning with a coordinate-sensitive photodetector comprising an LI-620 dissector (Elektron, Sankt Petersburg) and electronic unit. Usually, a single cell or part of it was seen in the visual channel. (b) Modulation of the reference wave phase $U(t)$ resulted in a change in the photocurrent intensity $I(t)$. The local phase value was found from the pulse length τ. The sampling periodicity and the image loading rate were determined by the modulation frequency (1 kHz or 1 ms per pixel). The noise-limited sensitivity was roughly $h_{\min} = 0.5$ nm.

invert and subtract snap-shots and map fluctuations, and to perform other procedures [42 – 31]. Programs of dynamic phase microscopy (DPM) allowed periodic measurements of the OPD on an arbitrary scan-line, their recording in the form of coordinate – time matrices (track diagrams), and representation of dynamic processes as spatio-temporal 'portraits.'

Interpretation of phase images is based on the generally accepted representation of an object as a spatially inhomogeneous optical medium with a refractive index $n(r, t)$ in a limited space region [11, 19]. As mentioned above, a serious problem is that the value being measured (OPD) in the eikonal [11] or geometrical optics approximation for a thin, transparent, and spatially inhomogeneous medium (e.g., a cell) depends inter alia on its physical thickness and refractivity, i.e., the difference between the refractive index $n(r, t)$ and that of the environment [11, 19 – 23].

Figure 2a shows a cell model in the form of a local inhomogeneity with transverse dimensions d and H. A wave from a coherent source passing through the cell undergoes front bending (spatial modulation) transformed in an interference microscope to an OPD or phase thickness distribution. This initial information is digitally coded in the topogram (Fig. 2b).

Figures 3a, b present the topogram and the cell thickness profile of a cell from human HCT 116 tissue culture along the selected section line. The pseudocolor topogram in Fig. 3a shows regions of different optical density and a contrast nucleus; the contour line depicts cell boundaries. In a typical section across the phase image of the unstained cell in Fig. 3b, the nucleus and nucleolus are fairly well distinguished by optical density (or phase thickness). The cytoplasm of the unstained cell in the phase thickness profile had a low, sometimes negative contrast. We recall that contributions of elements of the multilayer cell structure and various organelles are simultaneously projected onto the plane of the cell phase image in Fig. 2b. For this reason, the width of the region adjoining the cell border is much greater than the actual thickness of the cytoplasmic membrane. The phase thickness topogram and profile in Fig. 3 can be regarded as a certain generalized phase portrait of the cell [11, 28 – 31].

As mentioned above, the phase image in the (X, Y) plane viewed from the formal standpoint [11, 19] is a two-

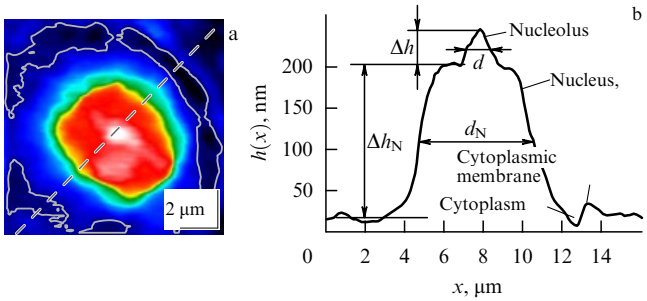

Figure 3. Phase image of a cell from the HCT 116 tissue culture. (a) The topogram shows a high-contrast nucleus and a lower-contrast cytoplasm – medium interface marked by a contour line. (b) Diametric section $h(x)$ through the phase image of an unstained cell exhibits a denser nucleus and nucleolus. The sizes shown in the phase thickness profile were used to compute the refractivity of the nucleus and nucleolus.

dimensional distribution of the optical path difference

$$h(X, Y, t) \cong h(x, y, t) = \int \left[n(x, y, z, t) - n_0\right] \mathrm{d}z\,,$$

depending largely on the difference between the refractive indices of the object $n(x, y, z, t)$ and the environment n_0. The optical path difference $h(X, Y)$ practically coincides with the phase thickness function in the object plane (x, y). The contrast of organelles in phase images of the cell increases with their refractivity Δn, which is equal to the mean difference between the refractive indices of the object $\langle n(x, y, z, t)\rangle$ and of the immersion medium n_0. However, this definition is inapplicable in real conditions in the absence of a priori information about the size of the inhomogeneity and the volume in which the mean value of $\langle n(x, y, z, t)\rangle$ was obtained. When averaging is performed over the entire object volume, the maximum phase thickness Δh can be represented as

$$\Delta h = \Delta n H = \left[\langle n(x, y, z, t)\rangle - n_0\right] H\,.$$

A more convenient and readily realizable approach based on an assumption about the object shape was used in MIREA to interpret results of interference measurements in terms of

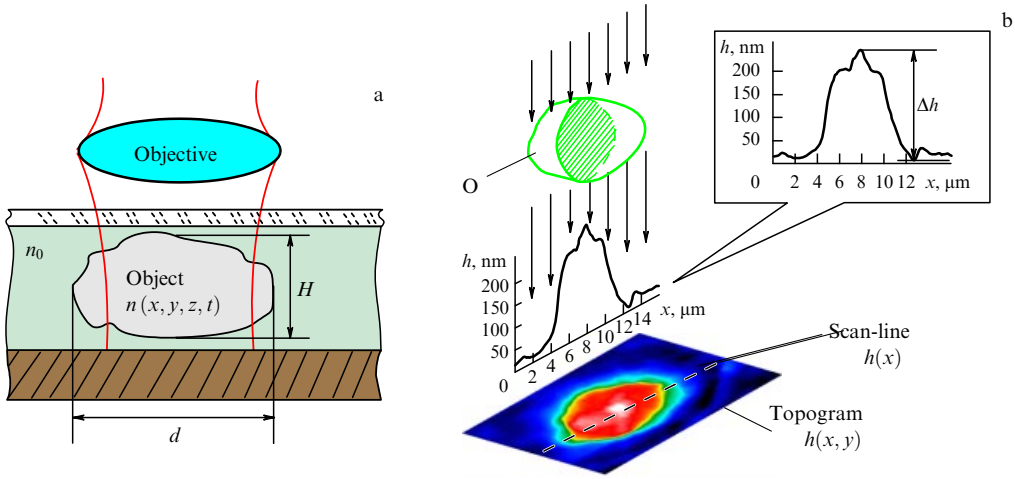

Figure 2. Optical model of a cell. (a) The object (cell) is represented by the optical inhomogeneity $n(x, y, z, t)$ in the ambient medium with the refractive index n_0. (b) The object modulates the incident plane-wave front. The modulated wave front is converted in the interference microscope into a topogram, i.e., a quantized two-dimensional distribution of the optical path difference $h(x, y)$ (phase thickness). The phase thickness profile $h(x)$ is derived from the section through the topogram along the scan line.

refractivity as a macroscopic parameter of the milieu. The available experience indicates that the approximation of spherical or cylindrical forms is in many cases correct, and the transverse size d measured in a phase image is an 'equivalent' of the geometric thickness H (see [19, 22] for a detailed discussion of this problem).

Here, the approximation $H \cong d$ [11] is used to determine the refractivity for which $\Delta n = \Delta h/H \cong \Delta h/d$, where Δh is the maximum phase thickness and d is the transverse size in phase images. Numerical values of mitochondrial refractivity obtained in this approximation were used to evaluate contributions to optical components of the electronic susceptibility (see below).

The Airyscan microscope permits registering dynamic processes in real time. Slow (of the order of minutes) variations in the object shape and thickness were apparent in a series of images obtained every 4 – 60 s (depending on the pixel number). Relatively rapid (0.001 – 1 s) fluctuations within a limited object region were registered by DPM [11]. The length of the scan line (Fig. 4a) and, accordingly, the number of pixels on it varied from 2 to 1024 and the maximum (Nyquist) frequency in the spectra from 0.5 to 250 Hz. The minimal pixel size for the Olympus 50*/0.75 lens was 12 nm.

Several methods were developed to localize metabolically active regions in the cell. Intense fluctuations usually occurred at steep segments of the phase thickness profile. Therefore, the scan lines on the topogram were chosen so as to intersect the cell putative active structure (e.g., nucleolus: see the diagonal in Fig. 4b). Measurements by this method took dozens of seconds. More laborious were measurements along the orthogonal grid lines fixed on the image, e.g., with a spacing of 1 μm (see the grid in Fig. 4b). Each consecutive line was scanned for 15 s. The groups of data in the form of a matrix $h(x, t)$ (see the filtered track diagram in Fig. 4a) for each scan line had the dimension 32×512 pixels (or 12 μm ×15 s). Measurement of one set of matrices (track diagrams) containing 20 sections per cell took 10 – 15 min. The method allowed the detection of intracellular 'signals' in the form of slow OPD changes and their 'mapping' and identification with concrete biophysical processes. Signals characterizing the functional state of cell organelles could be obtained from longitudinal sections of track diagrams (Fig.4a). Transverse sections displayed rapid changes in the phase thickness profile in response to external factors. Dispersion of the phase thickness values $h(x, t)$ served as a quantitative characteristic of the fluctuation intensity $I(x)$. Generally speaking, interpretation of the phase thickness fluctuations is less explicit because their association with morphological elements was unknown.

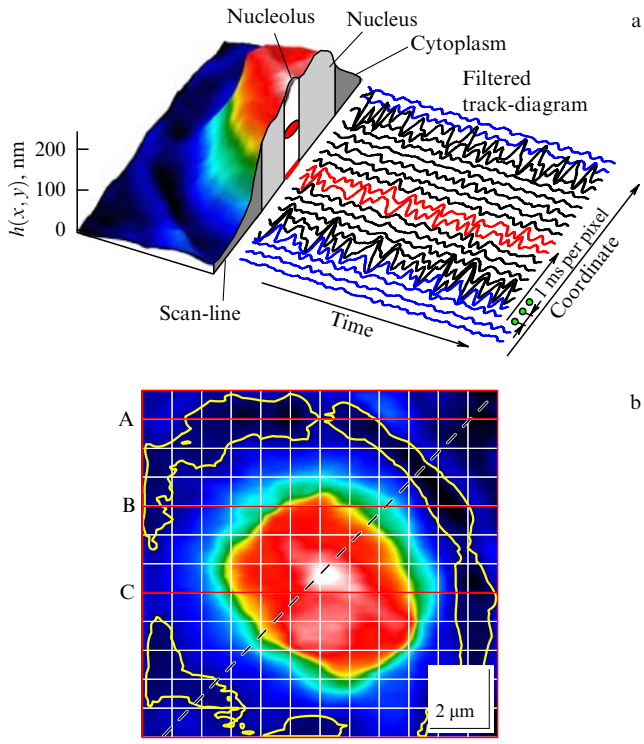

Figure 4. DPM method. (a) A single scan line or an orthogonal grid of scan lines was fixed in the cell phase image (topogram). Measurements of the phase thickness profile along the scan line at a fixed interval (from milliseconds to hundreds of milliseconds) were made periodically over dozens of seconds and loaded in the form of a matrix $h(x, t)$ (track diagram) into computer memory. (b) The section through the track diagram shows characteristic fluctuations in the vicinity of the nuclear membrane and in the nucleolus region.

4. Results of organelle and cell morphometry

The phenomenon of refractivity is traditionally used in microbiology to determine the functional state of spores [35]. In experiments carried out at MIREA, refractivity was used as a parameter coupled to mitochondrial energization; it was first reported to be dependent on the membrane potential in [24]. Further studies of chloroplast thylakoid membranes [25] demonstrated the dependence of refractivity on the proton concentration gradient ΔpH. Experiments with cyanobacteria *Synechocystis sp. PCC 6803* and spores of *Bacillus licheniformis* [26] also revealed the dependence of refractivity on energization, i.e., metabolic activity in a broad sense. It turned out that the metabolic component of refractivity in different biological objects naturally decreases with deenergization [24 – 26, 28 – 31]. It was hypothesized that alteration of energization is accompanied by a change in the state of certain water molecules. This simple model (see Section 6 and the Appendix) allowed deriving a formula for the normalized metabolic χ_3/χ_1 component of the medium susceptibility, which is in a sense a quantitative characteristic of energization and metabolic activity of a given biological object. Normalization of the metabolic component of refractivity yielded a more universal quantitative characteristic, the 'vitality' (see below).

The quantities Δh and d were derived from the phase thickness profile of biological objects. Deenergization of the objects resulted in characteristic changes in their phase images exemplified by alteration of the mitochondrial phase thickness [24] under the effect of rotenone inhibiting respiratory chain enzymes or ATP enhancing the membrane potential. Figure 5a shows phase thickness profiles of mitochondria in different media. Figure 5b illustrates the linear dependence of the average refractivity $\langle \Delta n \rangle$ on the membrane potential $\Delta\Psi$ found in measuring three populations of mitochondria in media of different compositions [24]. Rotenone substantially reduced refractivity to a minimum value $\Delta n \approx 0.01$. The highest refractivity values under ATP stimulation reached $\Delta n = 0.11 - 0.12$. The excess of refractivity $\delta n(\Delta\Psi) = \Delta n(\Delta\Psi) - \Delta n_{\min}$ over its minimum value ($\Delta n_{\min} = 0.01$) was designated as a metabolic component, and the difference between the extreme values $\delta n_{\max} = 0.10$ was regarded as the acceptable range of its variations. The

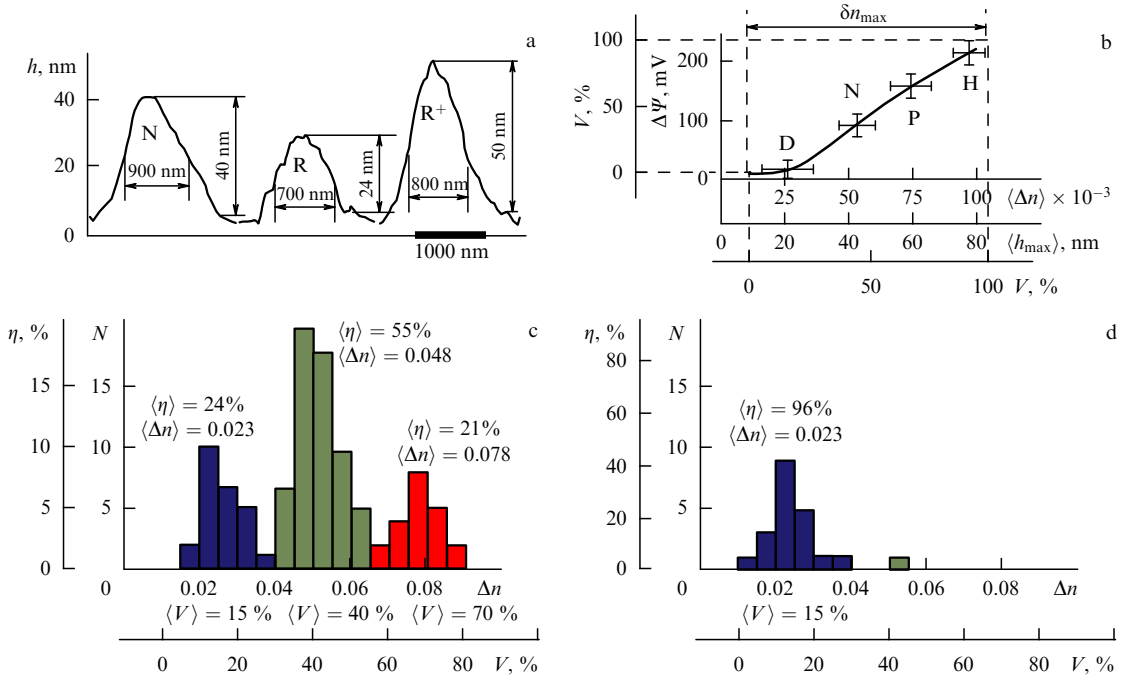

Figure 5. Effect of rotenone and ATP on mitochondrial refractivity. (a) Phase thickness profiles for intact (N), rotenone-inhibited, and ATP-stimulated (R^+) mitochondria. (b) Composition of the incubation-medium-influenced mitochondrial membrane potential ($\Delta\Psi$) and refractivity ($\langle\Delta n\rangle = \Delta h/d$)). The linear dependence $\langle\Delta n\rangle = \Delta n_{\min} + K\Delta\Psi$ was attributable to the electrooptical effect [24]. The difference $\delta n/_{\max} = \Delta n_{\max} - \Delta n_{\min}$ is defined as the maximum value of the metabolic component of refractivity. Normalization to the maximum membrane potential or $\delta n_{\max}$ allowed introducing the dimensionless parameter of 'vitality' $V = \Delta\Psi/\Delta\Psi_{\max} = \Delta n/\delta n_{\max}$ to characterize the cell state (see text). (c) Histogram of intact mitochondria shows three subpopulations differing in the mean refractivity ($\langle\Delta n\rangle = 0.023$; 0.048; 0.078). Normalization to $\delta n_{\max} = 0.12$ derived from the histogram allowed the 'vitality' value to be determined for each group. The second scale corresponds to a histogram renormalization for representing the results as values of V, %. Absolute values of realization numbers N are plotted on the ordinate along with their values normalized to $N_{\max}$, $\eta = N/N_{\max}$ (see the Appendix). The histogram of rotenone-inhibited mitochondria shows a single maximum $\langle\Delta n\rangle = 0.023$ ($V = 15\%$) with $\langle\eta\rangle = 96\%$.

additional left-side scale shows relative values of the membrane potential (V, %) normalized to $\Delta\Psi_{\max} = 220$ mV.

The results of measurements shown in Fig. 5b were used to generalize the conclusions to other objects whose membrane potential cannot be measured or whose functional state implicitly depends on other parameters, e.g., pH. In what follows, it is shown that under certain conditions, the parameter V arbitrarily referred to as 'vitality' may be used to characterize the state of an individual cell or organelle. Indeed, the linear dependence $\delta n(\Delta\Psi) = \Delta n(\Delta\Psi) - \Delta n_{\min}$ suggests the possibility of characterizing the state of mitochondria either by the parameter $V = \Delta\Psi/\Psi_{\max}$ or by the normalized metabolic component of refractivity (an excess over its minimum value $\Delta n_{\min}$). The metabolic component $\delta n/\delta n_{\max}$ normalized to the maximum value ($\delta n_{\max}$) can be interpreted (by virtue of the dependence $\delta n(\Delta\Psi)$) as an alternative definition of the relative membrane potential $V = \Delta\Psi/\Psi_{\max} = \delta n/\delta n_{\max}$. Examples of the 'vitality' parameter and the rationale for its application are discussed below (see also Section 6 and the Appendix). Figure 5c presents histograms for intact and inhibited mitochondria in the ordinary $N(\Delta n)$ and normalized $\eta(V)$ coordinates ($\eta = N/N_{\max}$ is the number of mitochondria in the range V, $V + \Delta V$). The histogram in Fig. 5c shows three subpopulations with the respective mean refractivity values $\langle\Delta n\rangle = 0.023$, 0.048, and 0.078; $\langle V\rangle = 15$, 40, and 70%; and 'weights' $\langle\eta\rangle = 24$, 55, and 21%. Comparison of histograms in Figs 5c and 5d indicates that rotenone increased the relative amount of low-energy mitochondria (from $\langle\eta\rangle = 24\%$ to $\langle\eta\rangle = 96\%$).

The generality of the observed dependence of refractivity and 'vitality' on the functional state is confirmed by measurements in objects of quite a different nature. Figures 6a and 6c present the results of measurements in cyanobacteria *Anabaena* indicating the mean refractivity $\langle\Delta n\rangle$ and vitality (energization) $\langle V\rangle$ decrease following a blockade of electron transport by DCMU or a 5-minute-long temperature shock (heating to 70 °C). The difference between the mean refractivity values in intact $\langle\Delta n\rangle_{\max}$ and deenergized $\langle\Delta n\rangle_{\min}$ cyanobacteria is apparent from histograms in Figs 6a and 6b. The effect of inhibitors on the normalized refractivity can be characterized as a decrease in the mean vitality of cyanobacteria from $\langle V\rangle = 60-70\%$ to $\langle V\rangle = 7-10\%$ of its maximum. Surprisingly, the refractivity changed very similarly in both cases, possibly due to the almost complete deenergization of all microorganisms. A similar approach was used to obtain the mean values $\langle\Delta n\rangle_{\max}$ and $\langle\Delta n\rangle_{\min}$ for cyanobacteria *Synechocystis*, bean chloroplasts, spores, and yeasts. From 20 to 50 measurements were made in each sample. The results of data treatment are presented in the table, together with the analogous findings for neurons (from [19]), HCT cell nuclei, and nucleoli [28–31].

The data in the Table illustrate the nontrivial fact of impaired refractivity in biological objects of different natures after their deenergization by various agents, as well as the surprisingly small difference between their minimal ($\langle\Delta n\rangle_{\min} = 0.01-0.025$) values. Low refractivity upon deenergization and, accordingly, the closeness of the refractive indices to $n_0 = 1.33$ for water suggest a relatively small contribution of 'dry' matter compared with that of

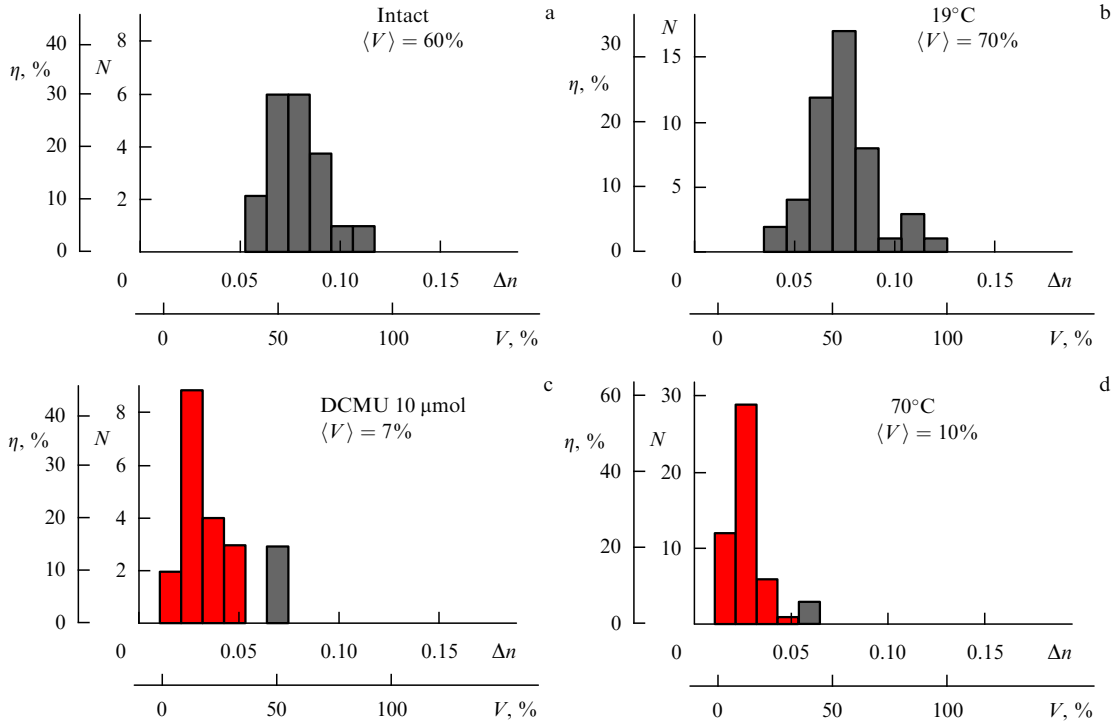

Figure 6. Effect of inhibitors on the refractivity and 'vitality' of cyanobacteria Anabaena. (a, c) Distribution histograms of intact and DCMU-inhibited bacteria illustrate a decrease in the mean 'vitality' from 60 to 7%. (b,d) Histograms of bacteria under normal conditions (19 °C) and after a high-temperature shock (70 °C) show a decrease in the mean 'vitality' from 70 to 10%.

Table. Effect of milieu on refractivity of biological objects.

Object	Deenergization factor	$\langle\Delta n\rangle_{\min}$	$\langle\Delta n\rangle_{\max}$	Energization	Literature
Mitochondrion	KCN, rotenone	0.02	0.08 – 0.1	ATP, succinate	[33]
Chloroplast	DCMU, nigericin	0.02	0.05	Intact	[31]
Synechocystis PCC 6803	KCN	0.025	0.07	Intact	[32]
Anabaena variabilis	DCMU	0.02	0.05	Intact	—
Intact — Spores *Bacillus licheniformis*	$T = 120\,^{\circ}$C	0.025	0.075	Intact - Spores	[12]
Yeasts	KCN	0.023	0.07	Intact	—
Nucleoli of HCT 116	Actinomycin	0.01	0.05	Intact	[12 – 14]
Nuclei of HCT 116 cells	Rotenone, SF6847	0.015	0.03	Intact	[34]
Neuron	Hypotension	0.032	0.042	Intact	[7]

Note: These data show a decreased refractivity of biological objects of different natures following their deenergization by various means and the closeness of their minimum ($\langle\Delta n\rangle_{\min} = 0.01 - 0.025$) values. The difference $\delta n = \langle\Delta n\rangle_{\max} - \langle\Delta n\rangle_{\min}$ is a characteristic of the metabolic component of refractivity.

water (see the Appendix). This finding is consistent with the high percentage of water content in biological objects. At the same time, a variation in the maximum refractivity values in a much broader range ($\langle\Delta n\rangle_{\max} \cong 0.03 - 0.1$) in intact objects is unusual and deserves a special discussion. It may reflect their individual properties, their prehistory, or a common characteristic of a given species related to the peculiar structure of the object. The 'norm' ($\delta n_{\max} = \langle\Delta n\rangle_{\max} - \langle\Delta n\rangle_{\min}$) is a characteristic of a specific group of objects. Also of importance is the inference (see the Appendix) that the respective metabolic component of susceptibility is in many cases significantly larger than the 'dry' one ($\chi_3 > \chi_2$) and depends on the functional state of the object.

A few comments are in order in addition to the data in the Table. The refractivity averaged over the ensemble decreased from $\langle\Delta n\rangle_{\max} = 0.05 - 0.08$ to $0.01 - 0.02$ in hepatic cell mitochondria placed in a hypotonic solution in the presence of cyanide or rotenone inhibiting the first respiratory chain complex. The maximum refractivity ($\langle\Delta n\rangle = 0.12$) was achieved by succinate supplementation or ATP stimulation [24]. An increase in refractivity in isolated chloroplasts [25] was induced by illumination following a short (1 – 5 min) period of darkness. Inhibitors of photosynthesis (nigericin)

and electron transport (DCMU) decreased the refractivity from $\langle\Delta n\rangle_{\max} = 0.04-0.05$ to $\langle\Delta n\rangle_{\min} = 0.02-0.025$. In cyanobacteria *Synechocystis PCC6803* [26], DCMU reduced the refractivity $\langle\Delta n\rangle_{\min}$ from 0.075 to 0.025. Resting spores of *Bacillus licheniformis* exhibited the highest refractivity ($\langle\Delta n\rangle_{\max} = 0.05-0.8$). It decreased to $\langle\Delta n\rangle = 0.01-0.02$ after autoclaving at $T = 120\,^{\circ}\mathrm{C}$ for 20 min. Less systematic measurements in Saccharomyces cerevisiae yielded $\langle\Delta n\rangle_{\max} \cong 0.065-0.075$. A blockade of respiratory chain enzymes by azide shifted the maximum by $\langle\Delta n\rangle \cong 0.025$. The mean cell diameter (ca. 4 μm) remained virtually unaltered.

Included in the Table are preliminary results of measurements in HCT 116 human cells (see below). They suggest the possibility, in principle, to use refractivity of nucleoli for the characteristic of the cell functional state.

The quantitative assessment of contributions to refractivity of the objects listed in the Table was made using an abstract model of biological objects in which the main components of the medium were water (index 1), dry residue (2), and a metabolic component (3), whose nature is considered below. It was shown (see the Appendix) that in deenergized mitochondria, the contribution of the dry component normalized to water ($\chi_2/\chi_1 \cong 7\%$) to the medium susceptibility was significantly smaller than the normalized contribution of the metabolic component ($\chi_3/\chi_1 \cong 18\%$). This paradoxical result for mitochondria and the analogous findings for other biological objects are quite surprising. Indeed, there is no sound explanation for the 'disappearance' of the material component in deenergized mitochondria equivalent to a decrease in the medium dry mass from 25 to 7%. This paradox can be more naturally and plausibly explained in terms of the hypothesis postulating an altered state (e.g., susceptibility and optical properties) of a medium constituent common to all biological objects under study. Such a characteristic component of living matter is certainly water. The mechanism of its contribution to the metabolic component of refractivity presents a fundamental problem (see Section 6).

5. Registration of intracellular metabolic signals

Measurements of the phase thickness $h(x)$ and fluctuation intensity $I(x)$ profiles in different sections of the orthogonal grid made it possible to locate high metabolic activity regions. The borderline between the cell and the medium in a phase image or in a phase thickness profile on the diametric section across the cell was distinguishable by virtue of a slight (3–5 nm) enhancement of phase thickness over a stretch of ca. 1 μm adjoining the cytoplasmic membrane. This region is enclosed by the contour line in the topogram in Fig. 3a (a projection of the multilayer cell structure). The 1–2-μm-long segment between the cell boundary and the characteristic steep slopes in the nuclear profile within which the local phase thickness decreased by 15–20 nm corresponds to the projection of cytoplasm. The negative contrast indicates that the cytoplasm refractivity was slightly negative ($-\Delta n \cong 0.002-0.004$). The cross section tangential to the cell boundary (along line A in Fig. 4b) is evidence of the local increase in the phase thickness naturally attributable to the long optical path in the denser part of the plasma membrane. The same region exhibits an insignificant increase in the local fluctuation intensity (not shown).

The diametric section through the cell (Fig. 7a; see also the horizontal scan line C in Fig. 4b) showed a substantially different phase thickness profile $h(x)$ with a readily distinguishable nucleus and more intense fluctuations $I(x)$ in the form of a broader dispersion of phase thickness variations. The profile $h(x)$ had a well-apparent peak of the phase thickness (up to 60 nm within a 1–1.5 μm length) against a relatively flat peak corresponding to the nucleus; this sharp increase in the phase thickness was identifiable with the nucleolus. The nucleolus was equally well distinguishable on the topogram, in the 3D cell image; its presence was confirmed by electron microscopy (data are not presented). The phase thickness profile at the sides of the nucleus was as steep as 0.2, its phase thickness being $\Delta h \cong 160-200$ nm and diameter $d \cong 8-10$ μm. We recall that the phase thickness proved to be dozens of times smaller than the real (geometric) one. The quantities Δh and d could be used to numerically assess the nuclear refractivity ($\Delta n_{\mathrm{N}} = 0.02$). The nucleolus refractivity was much higher ($\Delta n = 0.06$). This result is consistent with reports of a higher protein level in the nucleolus.

There are a variety of causes leading to phase thickness fluctuations, including technical ones. The local enhancement of the fluctuation intensity (up to $I(x) \cong 30\ \mathrm{nm}^2$) in the vicinity of the nucleolus was regarded as a manifestation of its metabolic activity discussed in more detail below. Here, suffice it to mention the nontrivial finding, a local increase in the fluctuation intensity to 150 nm^2 at the nucleus boundary, close to the nuclear membrane. The track diagram in Fig. 7c gives an idea of the character of the signals and their large (up to 20 nm) amplitude. The radial width of the active region measured some 1 μm, or an order of magnitude wider than the width of the nuclear membrane identifiable by electron microscopy. Signals at the opposite sides of the nucleus were partly anticorrelated (see lines indicated by double arrows). Anticorrelation of phase thickness fluctuations in the nuclear membrane could be a consequence of the changes in both the diameter and the motion of the nucleus. It appears from Fig. 7c that fluctuations in the nucleolus phase thickness (tracks in the middle) had a different shape and amplitude and did not correlate with nuclear membrane fluctuations. The character of signals on track diagrams and intense spectral components in the limited frequency range 0.3–2 Hz as shown in Fig. 7d suggest their nonrandom nature. This inference was confirmed in experiments with the use of inhibitors. For example, the addition of 0.25 μmol actinomycin D (DNA blocker) resulted in a decrease in the fluctuation intensity by one order of magnitude (to 6–8 nm^2) within 25 min and the disappearance of contrast components from the spectrum (data are not presented).

Measurements within a small segment of the section tangential to the nuclear boundary (see scan line B in Fig. 4b) using an Olympus 50*/0.75 objective (i.e., at a higher resolving power) revealed the presence of small-scale structures. Figure 8a shows a structure with the characteristic transverse size 50–100 nm in the phase thickness profile $h(x)$. Figure 8b illustrates a local (70–100 nm) increase in the fluctuation intensity $I(x)$ at a different segment of the scan line in the vicinity of points $x = 0.5$ and 1 μm. It follows from the spectral portrait in Fig. 8c that the contrast spectral components with the frequencies $F = 0.15$, 0.5, 0.8, 1.2, 1.8, and 2.3 Hz in the vicinity of the point $x = 1$ μm had a very small length (70–100 μm) along the scan line. The spectral density of individual components amounted to 2,000 $\mathrm{nm}^2\ \mathrm{Hz}^{-1}$ (Fig. 8d) and was higher than that on the diametric section shown in Fig. 7d. This means

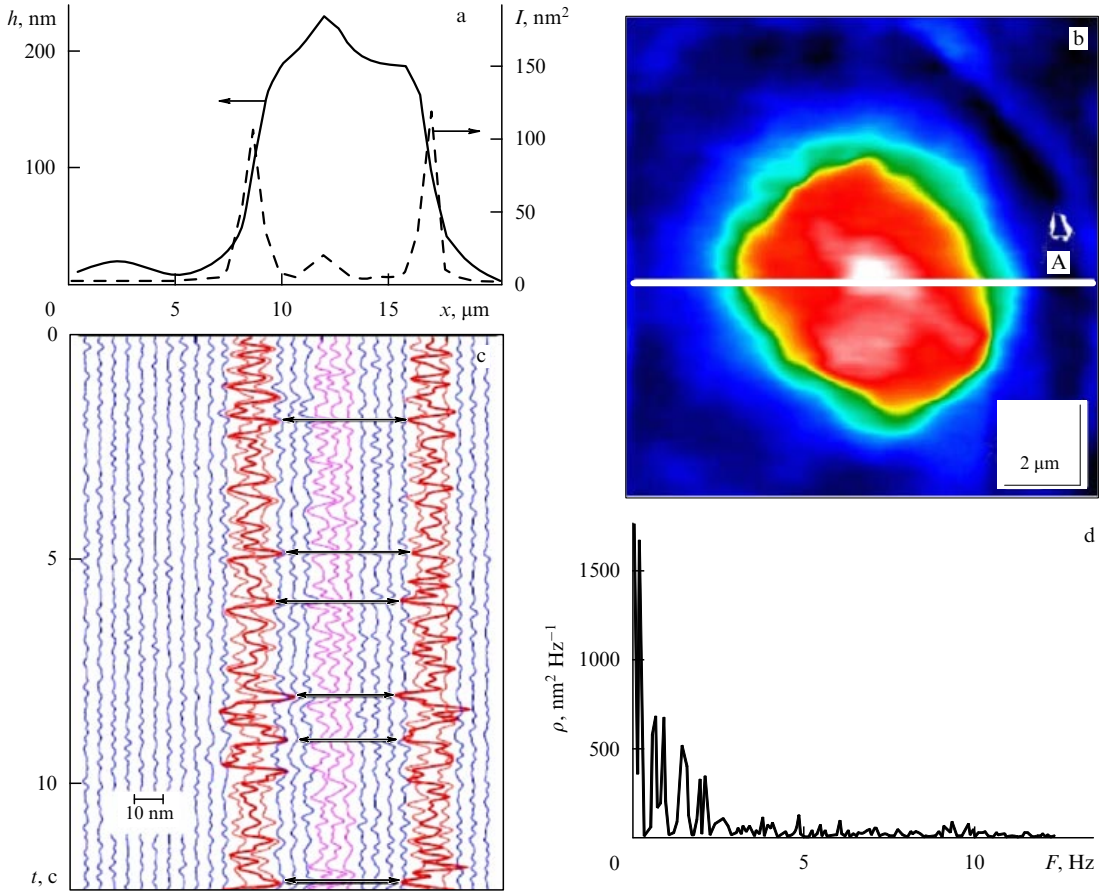

Figure 7. Phase thickness and fluctuation profiles in the diametric section through a cell. (a) The phase thickness profile $h(x)$ in the section along scan line A shows the nucleolus as a local thickening against a background of the nucleus. Intense fluctuations $I(x)$ were regularly observed at nucleus boundaries and in the nucleolus region. Experiments with inhibitors confirmed the metabolic origin of the fluctuations. The radial width of this active region is an order of magnitude greater than the width of the nuclear membrane measured by electron microscopy. (b) The topogram of the cell shows the correlation of nucleus and nucleolus images with the phase thickness profile. (c) Large (up to 20 nm) fluctuation amplitudes with repeated characteristic structures on the track diagram were found close to the nuclear membrane. Somewhat smaller amplitudes could be seen in the vicinity of the nucleolus. Points of pronounced anticorrelation at the opposite sides of the nucleus are shown by the double arrow. (d) Fluctuation spectra at the nucleus boundaries exhibit intense contrast components in the frequency range 0.3 – 2 Hz.

that fluctuations in the diametric and tangential sections were due to different causes. The nonstationary character of the processes, their spatial correlation, and the characteristic shape of the signals with an amplitude as large as 20 nm can be seen on the track diagram in Fig. 8e. The length of certain signals indicated by the asterisk on the scan line was large (up to 1 μm) and exceeded the width of the active region in Figs 8b, c. The lines passing through their characteristic points had a noticeable slope ($\approx \pm 1$ μm s^{-1}), which remains unexplained. The local fluctuations in the vicinity of putative pores may be associated with protein and pre-ribosome transport (see Section 7).

We briefly consider a potential mechanism underlying these signals. As is known, the nucleolus is a highly organized organelle containing a large number of small interconnected fibrillar centers with a different degree of rDNA condensation and a less compact granular component [36 – 42]. The picture of the nucleolus in the phase thickness profile (Fig. 7a) and the track diagram of its fluctuations (Fig. 7c) obtained under low magnification (with an Olympus 20*/0.4 lens) do not reflect all the peculiarities of its structure and dynamics. Minor structural details and their changes in time became noticeable under high magnification (using Olympus 50*/0.75). The dynamics of the nucleolus were apparent as variations in its size, shape, and phase thickness for a few minutes. Certain nucleoli underwent internal structural changes. The section through the nucleolus in Fig. 9a displays a local 15 nm increase in the phase thickness in the region with the transverse dimension ca. 300 nm. Correlated spatio-temporal fluctuations with characteristic repeated structures ('events') could be seen on the section through this thickening shown in a detail of the track diagram in Fig. 9b. The intensity of fluctuations ($I(x)$ in Fig. 9c) varied sharply over the cross section and amounted to a maximum of 35 nm^2 at the border with the thickening believed to correspond to the projection of the dense fibrillar component. The long low-frequency (0.2 – 0.7 Hz) and short (up to 50 nm, 0.7 – 1.5 Hz) components in the spectral portrait shown in Fig. 9d corresponded to local processes in the vicinity of the intensity maximum within the 300 nm region. The extent of events along the scan line in the track diagram in Fig. 9e varied in a broad range (50 – 400 nm). The metabolic nature of the events was confirmed in experiments with inhibitors. Small (<0.1 μmol) concentrations of actinomycin D induced marked changes in both morphology and signals [28 – 31]. Fluctuations stopped within a few minutes and resumed after 30 – 40 min. High concentrations of actinomycin (0.6 – 1.0 μmol) caused irreversible changes to the profile and

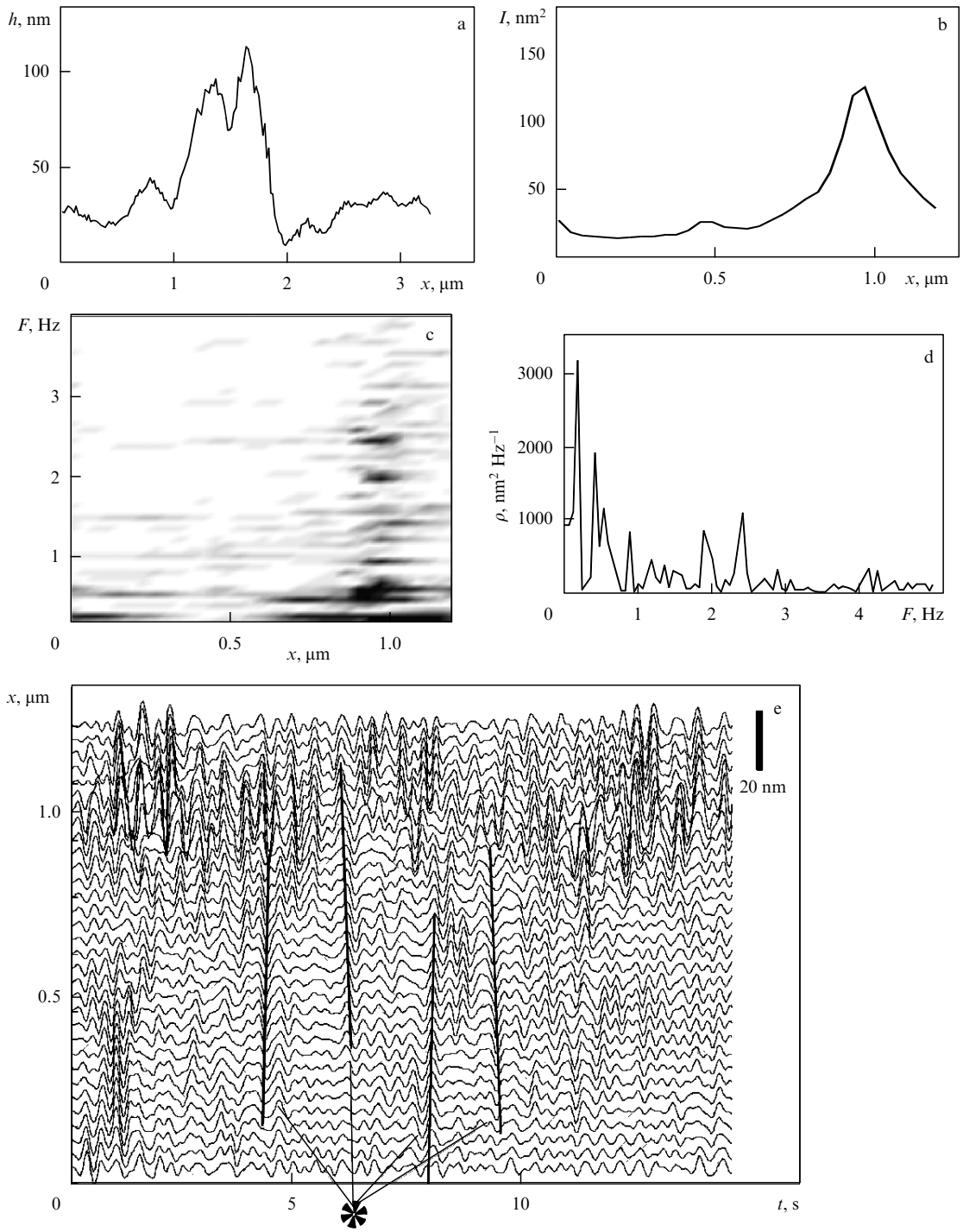

Figure 8. Fluctuations in the section tangential to the nucleus boundary. (a) 100 nm structures similar in size to a nuclear pore were observed in the section along scan line B in Fig. 4b. (b) Local (~ 100 nm^2) enhancement of the phase thickness fluctuation intensity in scan-line segments in the vicinity of points $x = 0.5$ and 1 μm. (c) Contrast short-length (70 – 100 nm) components along the scan line are visible in the frequency range $F = 0.15 - 2.5$ Hz in a detail of the spectral portrait in the vicinity of the putative pore ($x = 1$ μm). (d) Contrast components with a high spectral density are well apparent in the vertical section through the spectral portrait at the point $X = 1$ μm. (e) Nonrandom signal shape with characteristic repeated structures of different length along the scan line in the vicinity of the putative pore may be due to phase thickness variations during protein and pre-ribosome transport. The lines indicated by the asterisk correspond to processes with a large correlation radius.

fluctuations (not shown). These findings indicate that fluctuations in OPD in the nucleolus are directly or indirectly associated with rDNA transcription and pre-ribosome synthesis [36 – 42].

The results of the measurements were interpreted with the help of the models described in the literature [36 – 39] and numerical assessments of the synthetic rate [38 – 41]. According to the current concepts [39 – 41, 43 – 45], thousands of pre-ribosomes are simultaneously synthesized on a score of transcriptional units within each cluster about 0.01 μm^3 in volume. Over one hundred rRNA polymerases (Pol I) on each transcriptional unit consecutively initiate and complete the synthesis of giant 45S precursor molecules with the mass 4.6×10^6 Da. Synthesis of a single 45S particle lasts from 150

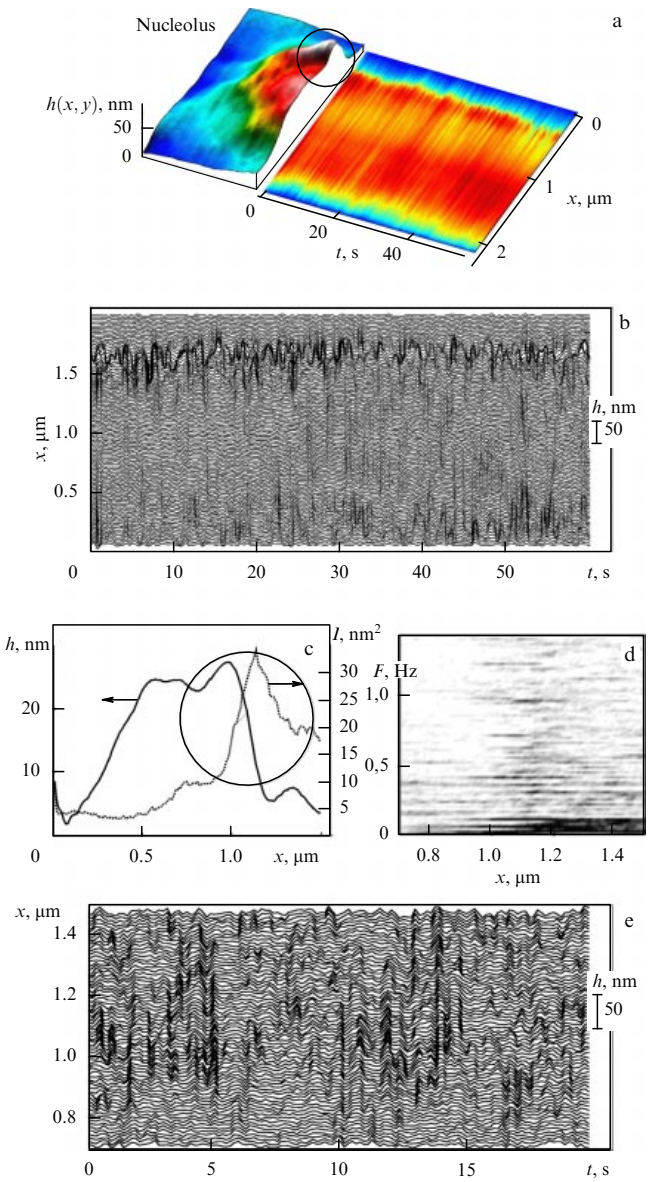

Figure 9. Fluctuations in the vicinity of the nucleolus. (a) Details of the spatial structure could be seen in the nucleolus within a field of 2×2 μm^2 under high magnification (Olympus 50*/0.75). A local increase in the phase thickness (transverse size ca. 300 nm, inside the circle) presumably corresponds to the dense fibrillar component that bounds the granular component; the borderline between them is the site of pre-ribosome synthesis. The position of the scan line was chosen such that it allowed recording fluctuations associated with the putative processes of transcription and synthesis. (b) The track diagram shows spatio-temporal correleation and locality of fluctuations with repeated structures ('events') of different lengths along the scan line. (c) Position of the active region where the fluctuation intensity $I(x)$ reached 35 nm^2 relative to the steep slope in the phase thickness profile $h(x)$. The intensity was 3–4 times lower in the remaining portion of the nucleolus (supposedly its granular component). (d) The detail of the spectral threshold demonstrates the predominance of long low-frequency ($F = 0.2-0.7$ Hz) components in the active region and the small (up to 50 nm) length of higher-frequency components ($F = 0.7-1.7$ Hz) along the scan line. (e) The track diagram of the active region shows 'signals' of a characteristic structure supposedly associated with pre-ribosome synthesis.

to 300 s; it separates from the transcriptional unit after a lapse of 1–2 s and translocates to the granular component region. The following processes occur during each period $T \cong 1-2$ s [36–45]: self-assembly and initiation of Pol I, elongation of pre-ribosomes via binding of all Pol I to amino acids, Pol I dissociation, termination of synthesis, and separation of the finished pre-ribosome. Obviously, the motion of an entire ensemble of a large number of Pol I must be synchronized, within each transcriptional unit at least, although direct evidence of such synchronization remains to be obtained. It should be noted without going into details of the pre-ribosome synthesis (e.g., time-correlated escape of pre-ribosomes to the granular component region) that the mean period of initiation on the transcript is close to $T \cong 1.4$ s, which corresponds to the frequency 0.7 Hz [39–41, 43–45]. It appears from the spectral portrait in Fig. 9d that fluctuation frequencies in the active region of the nucleolus (within a cluster) are close to this value and lie in the range 0.2–1 Hz. The agreement between the values is hardly a mere coincidence, and the result is consistent with the scenario described below.

A dozen 'conveyors' simultaneously work in each cluster of the nucleolus active region where ensembles of Pol I move synchronously. The presence of nonrandom intense signals and contrast components with frequencies up to 1 Hz in the nucleolus is consistent with synchronous Pol I motion and indicates at least reciprocal influence and partial synchronization of the processes between individual conveyors. Apparently, macroscopic changes in phase thickness associated with these cooperative processes are the most likely cause of fluctuations observed in the nucleolus.

In the proposed scenario, small-scale (50–70 nm) events within the active region in the track diagram in Fig. 9b and in the spectral portrait in Fig. 9d are assignable to the work of individual transcriptional units. Certain (a few) events of long duration may be due to the motion of the entire cluster and/or cooperative movements of its several transcriptional units [42, 43]. The position of the cluster identifiable with the center of events could vary within the active region.

Rhythmic patterns of the above processes give enough grounds for the physical interpretation of the 'signal' origin at a qualitative level. For example, they can result from conformational transitions in Pol I responsible for regular changes in the optical density in macroscopic volumes of the cluster. It is worth noting that a 20 nm change of the phase thickness in a cluster measuring some 200 nm may be caused by a local change in refractivity by 0.1. Certainly, the transcription and synthesis processes are very complicated, and there are no means yet to distinguish between their contributions to the events associated with the rhythmic work of conveyors. For all that, reproducible structures of the signals and other signs of the universality of events suggest their relation to fundamental processes. The discussion of specific mechanisms of the dependence of optical parameters on the functional state of cells and organelles is beyond the scope of this paper.

6. Mechanisms of the metabolic dependence of refractivity

Successful application of the proposed methods depends on the understanding of a fundamental biophysical problem, the dependence of refractivity on metabolism. There are at least several hypotheses explaining this universal mechanism, but an explanation is hampered by the lack of data on the metabolic dependence of refractivity [19–31] and by the still poorer knowledge of its nature. Three models are conceiva-

ble, arbitrarily referred to as hydrate, conformational, and structural. The most attractive hydrate hypothesis of the mechanism of the metabolic component of refractivity is based on the following facts:

(1) The cessation of metabolic processes leads to a decrease in the electrochemical potential $\Delta\mu = \Delta\Psi + \Delta\mathrm{pH}$ and/or a change in the protein charge state, e.g., during the coil/globe transition of chromatin to a condensed state in high-ionic-strength solutions.

(2) The refractive index in electrolyte solutions increases with increasing the ion concentration due to the appearance of ionized water molecules in the hydrate membrane having a higher-ordered orientation of dipole moments (see, e.g., [46]).

The proposed hypothesis is based on the fact that cessation of metabolism is accompanied by a decrease in the ion concentration in a biological object and charge density on its cytoplasmic membranes. This mechanism, especially characteristic of biological objects with a well-developed membrane system, is operative in cyanobacteria, mitochondria, and a few other organelles. Part of the water molecules near the charged membrane surface is in the bound state (Fig. 10a), being characterized by enhanced electron polarizability compared with ordinary water molecules. This property is manifested as a decrease in the refractive index averaged over the volume during deenergization (see the Appendix). The universal character of such an explanation for the metabolic dependence of refractivity ensues from the fundamental nature of the aforementioned biological and physical laws (see pp. 1 and 2). The layer of bound water molecules is very thin and direct measurements of its polarization are virtually impossible. Nevertheless, there are a few indirect positive arguments. For example, measurements on phospholipid membranes [47] confirmed the important contribution of water to the dependence of refractivity on the potential gradient. The complexity of the problem under discussion and its debatability preclude proposing a rational alternative to the hydrate hypothesis for explaining the predominant contribution of water molecules to refractivity. This problem is discussed at greater length below.

Numerous publications on water properties are virtually lacking in data on the contribution of water molecules to the refractivity of biological objects [48 – 54]. Equally scarce are results of measurements and other evidence of the relationship between changes in the refractive index of biological objects and charge generation and/or the concomitant contribution of their hydrate membrane. On the other hand, it is known [48 – 50] that the fraction of oriented water molecules increases close to the hydrophilic surface of biological membranes.

The effect of surface charges on the structure of hydrogen bonds in water molecules is of a general character as manifested in molecular vibration spectra. Hydroxyl vibration spectra in a thin water layer near the charged membrane surface always contained a broad 3200 cm^{-1} band inherent in free water molecules with a complete set of hydrogen bonds in the tetrahedral configuration. But the intensity of another band in the vicinity of 3400 cm^{-1} depends on ion concentration [48 – 50], and its appearance was attributable to the partial break of hydrogen bonds or distortion of their asymmetric configuration [48]. This means that the polarized state of a fraction of water molecules depends on charges at the lipid membrane surface. Moreover, some authoritative researchers report other indirect arguments in favor of the proposed hypothesis. The water problem and the related

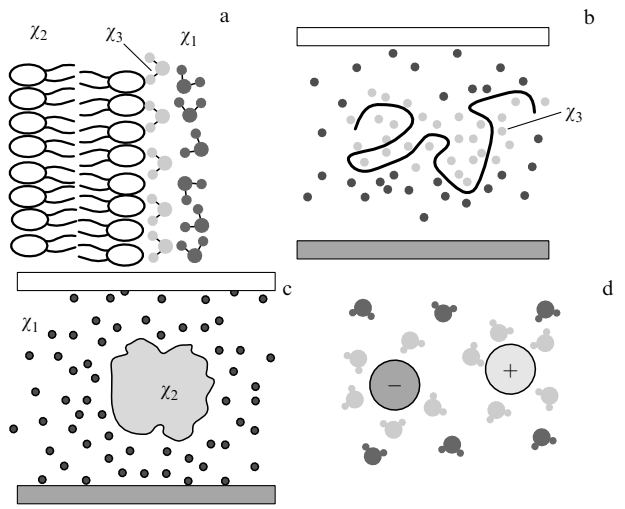

Figure 10. The mechanism underlying the appearance of the metabolic component of refractivity. (a) The thin layer near the charged membrane surface of water molecules (gray circles) has ordered orientation of dipole moments and an apparently higher electron component of sensitivity χ_3 than free water molecules (χ_1, black circles). The contribution of membranous protein structures and other 'dry' components of organelles to the electron polarizability is denoted by χ_2. (b, c) Transition of a protein macromolecule to the condensed state significantly decreases the number of charge-bound water molecules and the contribution of the χ_3 component. Because practically all metabolic processes (gene transcription, RNA translation and synthesis, DNA replication) are accompanied by alteration of the protein conformation, this change can be manifest as slow or rapid fluctuations of refractivity. (d) Water molecules in ion hydrate membranes have an ordered orientation of dipole moments, partly broken hydrogen bonds, and apparently enhanced polarizability.

anomalies being of paramount importance, here are a few facts and quotations.

Cremer [48] writes: "... Interfacial water molecules are highly ordered in comparison to bulk water and their particular structure depends on the prevailing pH. ⟨...⟩ Various ions are able to make and break hydrogen bonds."

Cheng [49]: "... The water molecules bound to the bilayer surface are less hydrogen-bonded and exhibit a higher vibration frequency than bulk water."

Wiggins [51]: "If water, somehow, locally changed its density so that its hydrogen bonds became straighter and stronger or bent and weaker, all its physical and chemical properties must change. ... Ling [52] had recognized this problem and proposed that intracellular water existed as polarized multilayers at protein surfaces, thus providing adequate volumes of modified water. At protein surface, some water molecules must interact directly to hydrate the surface." (In this respect, the hypothesis being considered is consistent with the 'polarized multilayer theory of protoplasmic water in living cells' suggested by Ling [52].

Chaplin [54] analyzed over one thousand publications (see, e.g., [48 – 54]) on anomalous water properties. His review demonstrated that many intracellular biochemical processes may affect the configuration of water molecules and their macroscopic parameters.

The second (also universal) mechanism of the metabolic component appears to be related to the conformation (folding) of protein macromolecules [55, 56]. The folding occurs in practically all metabolic processes. For example, translation of mRNA leads to lengthening the polymer amino

acid chain, which spontaneously turns into a more compact stable structure (Figs 10b, c).

Protein folding in solutions proceeds via a series of intermediate states, with the protein charge configuration and the interaction of its polar groups with water molecules playing a key role. Compact configurations correspond to a free-energy minimum and a minimum part of the hydrophobic surface that is in contact with water molecules. In contrast, polar groups tend to localize at the outer surface of a given structure and interact with water. Figure 10b, c schematically shows a decrease in the number of protein-bound water molecules in the 'condensed' state. The fact of the dependence of a fraction of broken hydrogen bonds on the protein spatial structure, conformation, and charge state and on the medium pH is paramount for the qualitative explanation of intranucleolar and intranuclear effects in the framework of the hypothesis under consideration. Ions have a characteristic hydrate membrane with bound water molecules (Fig. 10d), and an increase in their concentration in cytoplasm and nucleoplasm may also contribute to the metabolic component of refractivity. Because gene transcription, RNA translation and synthesis, DNA replication, and practically all other metabolic processes are accompanied by alteration of the protein conformation, changes in the structure of macromolecules and the number of broken hydrogen bonds must affect the integrated refractivity of the medium. Folded (deenergized) protein molecules contain fewer open polar groups; therefore, the integrated refractivity must be reduced. This inference agrees with the reduced nuclear refractivity in deenergized cells [30, 31].

Almost all works on the protein structure and folding [55, 56] report the dependence of the hydrate membrane on the conformation, the functional state, the ionic strength of the solution, and many other factors. In particular, the number of bound water molecules decreases as the compactness of DNA packaging increases, leading to the arrest of RNA transcription and translation. Despite the complexity and multifacetedness of these processes, there is little doubt that alteration of the DNA hydrate state is related to cell deenergization. To cite M. Chaplin, a known expert in protein hydrate membranes, "the extensive surface of cellular membranes (up to 100,000 um^2) favor the formation of low density water inside the cell. The membrane lipids contain hydrophilic head groups that encourage the organization of the assisted interfacial water. ... There is generally an ordered structure in the layer of water molecules immediately surrounding the protein, with both hydrophobic clathrate-like and hydrogen-bonded water molecules each helping the other to optimize water's hydrogen bonding network. Protein carboxylate groups are generally surrounded by strongly hydrogen-bonded water whereas the water surrounding the basic groups arginine, histidine and lysine tends towards a more open clathrate structuring" [54].

Finally, the third sufficiently universal mechanism of the metabolic component relates to the optical anisotropy of macromolecules contained in cytoplasm, nucleoplasm, and practically all other intracellular organelles. The structure of these organelles is known to resemble that of liquid crystals [57] with its optical anisotropy and phase transitions. Equally well known are electrooptical effects in liquid crystals, e.g., a change in the refractive index under the action of an external electric field [57]. Therefore, variations in the membrane potential, pH, protein conformation, and other factors accompanying metabolic processes may induce second-order phase transitions or changes in the susceptibility tensor components and the refractive index.

The problem of the dependence of refractivity on the origin and functional state of 'signals' is not confined to the above mechanisms. All known processes of medium polarization are inertial, and it is impossible to predict a priori how quickly refractivity will 'react' to, say, changes in the membrane potential. The inertia of polarization processes and the related dipole orientation may be a factor limiting the informative value of signals because their amplitude must decrease with increasing the frequency. Not surprisingly, fluctuation spectra are dominated by low-frequency components ($F < 10$ Hz). Of course, this does not exclude the existence of faster processes, but their registration will require a different approach.

In conclusion, there is an important problem of the interplay between signals and the spatio-temporal correlation of metabolic processes. Movements of individual macromolecules are indistinguishable because of a limited spatial resolution even if their signals have sufficiently large amplitudes. Interference methods differentiate only between macroscopic changes in the medium polarization; hence, the necessity to consider fundamental factors limiting the minimum volume of a medium in which refractivity variations can be discovered in the form of an optical signal.

If the signal is to be detected, this volume ΔV must contain correlated spatio-temporal changes in the refractivity with the amplitude δn. In this approximation, it is possible to determine the minimum value of the product $\delta n \Delta V$ as a signal with the amplitude $\delta h = (\Delta V \delta n)/S$ exceeding the limiting sensitivity $\langle \Delta h \rangle$ of the measuring device at a given spatial resolution S (see the Appendix). This means that interference methods permit detecting only signals related to macroscopic changes in medium parameters and induced by cooperative processes in cells and organelles [11, 27].

7. The problem of cell 'language,' 'dialogue,' and the biological interpretation of signals

The 'dialogue' with an object underlies biological structure–function experiments designed to derive information on metabolic processes (functions) from data on the morphological structure of the object of interest. Direct signal recording, e.g., in the form of fluctuations in the membrane potential [4, 5], is equivalent to introducing a new dimension or information channel in the signal–structure–function scheme. A temporal signal not only substantially extends the possibilities for 'communication' with the object but also ensures a higher level of the interactive real-time dialogue. We recall that by a signal (in the general case) we mean all characteristic features of the spatio-temporal structure regardless of their physical nature. In particular, it may be a video or audio signal recorded by methods other than optical interference microscopy. In the present concrete example, the signal is represented on the track diagram as fluctuations in the phase thickness. The nontriviality of the proposed 'semantic' approach is reflected in the hypothesis according to which signals recorded in real time contain objective and meaningful information in the cell's 'language' intelligible to the experimenter. By language we mean a totality of characteristic features in the signals allowing them to be distinguished and identified with specific intracellular processes. The problem of distinguishing and interpreting signals needs an interdisciplinary approach to be settled; effective

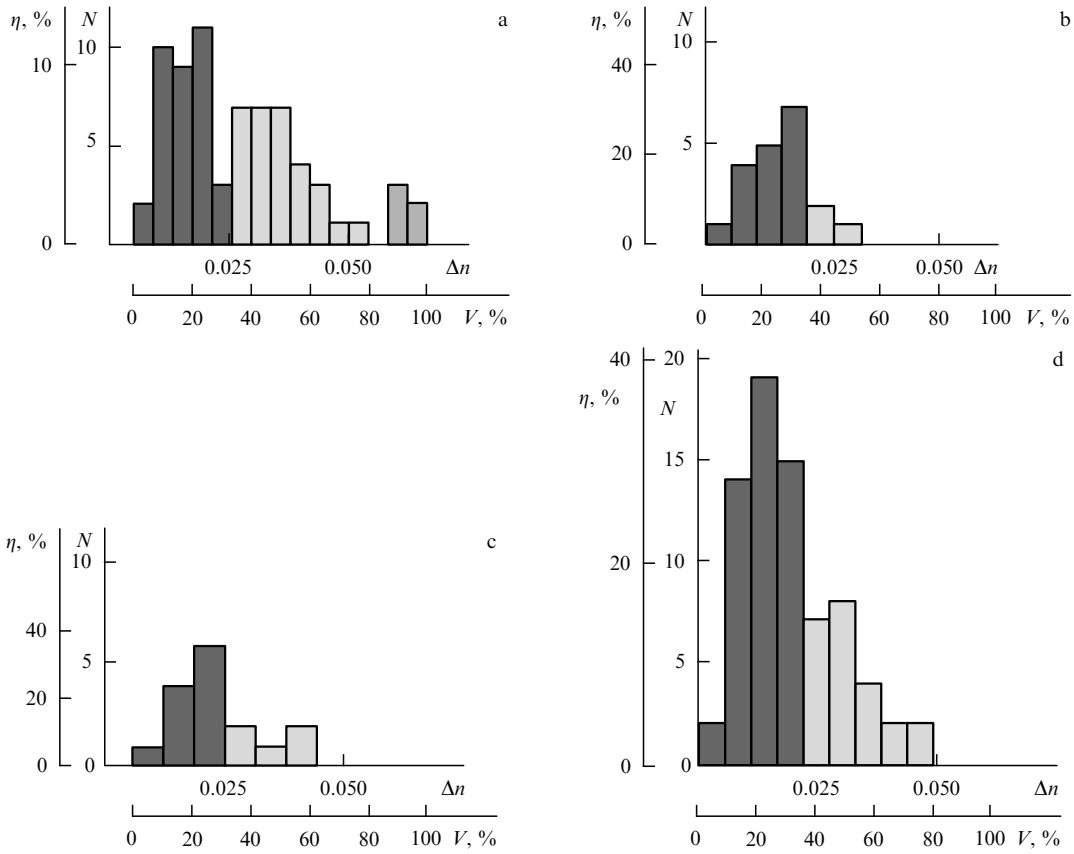

Figure 11. The effect of inhibitors on the refractivity of nucleolus and 'vitality' of HCT 116 cell subpopulations. (a) The histogram of intact cells exhibits three subpopulations with relative 'weights' η, the mean refractivity $\langle \Delta n \rangle$, and the relative vitality $\langle V \rangle$. (b) Aphydicolin eliminated the active subpopulation and increased the number of low-activity cells to $\eta = 85\%$. (c) Rotenone and decoupling agents inhibiting mitochondrial respiratory chain enzymes and ATP synthesis had a similar effect. Also, they arrested energization of metabolic processes. (d) Vincristine inhibited synthesis of microtubules through which proteins are transported to the nucleus. This led to an increase in the number of low-refractivity cells.

instrumental and technical means have been developed for its solution in individual disciplines. Suffice it to point to the problems of real-time interpretation from one language into another, prediction of earthquakes, and analysis of encephalograms. Unambiguous identification of signals with specific metabolic processes in a study object requires a 'dictionary,' for whose creation no means have thus far been suggested. The dictionary problem is complicated by the variability of cell conditions depending on the cell cycle phase, energization level, previous history, and other individual traits. Therefore, the dictionary, adequacy, and nonambiguity of its terms needs a separate discussion. Also, the idea of using refractivity as an adequate parameter describing the functional state of the cell is sometimes met with opposition.

For all that, concrete decisions can be proposed in certain situations. Cell biophysics employs a variety of methods to influence the functional state of the cell, making it possible to alter signals related to concrete cooperative processes. A specific case can be illustrated by the above example of signals produced in the nucleolus. It was mentioned above that the principal function of the nucleolus (pre-ribosome synthesis) is realized in the course of a cooperative process, i.e., synchronous motion of hundreds of RNA polymerases I (see reviews [37 – 44]). Other processes in the nucleolus appear to be unrelated directly to transcription and synchronism of Pol I. This fact substantially simplifies identification of signals with the functional state of the nucleolus and allows the quantitative comparison of their characteristics with data obtained by alternative methods. Preliminary results of experiments with actinomycin D (inhibiting transcription), aphydicolin (inhibiting DNA replication), and vincristine (inhibiting microtubule synthesis) demonstrated a correlation between phase images and the functional state of HCT 116 cells [29].

To conclude, here are the results of preliminary studies that confirm the reality of interpretation of nucleolus phase images. As is known, the intensity of synthetic processes in the nucleolus is one of the indicators of the cell functional state [37 – 42]. Active pre-ribosome synthesis, e.g., in tumor cells, is associated with enhanced nucleolus size and contrast. Measurements performed at MIREA confirmed the correlation between the nucleolus refractivity and the functional state of the cell. Figure 11 shows histograms of the nucleolus refractivity in intact and inhibitor-treated cells. Intact HCT 116 cells (Fig. 11a) were represented by three subpopulations with the refractivity $\langle \Delta n \rangle \cong 0.015$, 0.035, and 0.065; 'vitality' $\langle V \rangle \cong 15$, 50, and 90%; and nucleolus 'weight' $\eta_\Sigma = 50$, 43, and 7%. Only two subpopulations remained after inhibition of DNA polymerase and chromosome replication by aphydicolin ($\langle \Delta n \rangle \cong 0.015$ and 0.025; $\langle V \rangle \cong 30$ and 45%; $\eta_\Sigma = 85$ and 15%, respectively). A blockade of the first complex of the mitochondrial respiratory chain by rotenone and decoupling agent SF6847 resulted in two subpopulations with $\langle \Delta n \rangle \cong 0.015$ and 0.03; $\langle V \rangle \cong 20$ and 50%; $\eta_\Sigma = 70$ and

30%. Vincristine inhibiting polymerization of microtubules also affected the refractivity of nucleoli. The subpopulations had the respective parameters $\langle \Delta n \rangle \cong 0.012$ and 0.03; $\langle V \rangle \cong 20$ and 55%; $\eta_\Sigma = 70$ and 30%. Results of these preliminary measurements suggest the possibility of a quantitative assessment of the cell response to cytotoxic agents. It remains to be elucidated why different inhibitors induced a virtually identical response.

Finally, there is an issue of a parameter adequate to the problem of assessment of the state (energization) of the cell and its organelles. This macroscopic parameter of a biological object must have a clear physical interpretation and an understandable mechanism of the metabolic dependence. One of the main results in the present work is the introduction of the notion of the metabolic component of the susceptibility parameter (χ_3 or the refractivity $\delta n = \langle \Delta n \rangle_{\max} - \langle \Delta n \rangle_{\min}$) for the quantitative characteristic of the cell functional state. This parameter is amenable to direct, almost noninvasive optical measurement. In this sense, the metabolic component of the refractivity is an alternative to and a quantitative characteristic of a less concrete term 'energization.' It follows from Figs 5, 6, and 11 that the parameters $\langle \Delta n \rangle$, $\langle V \rangle$, and η_Σ may also characterize the population heterogeneity. Representation of histograms in the $\eta(V)$ coordinates may prove helpful for the quantitative assessment of the efficiency of the action of external factors, diagnosis of intermediate states, nonuniform distribution, etc. Advantages of such a representation include the possibility of performing real-time measurements and disregarding the mechanism underlying the metabolic dependence of refractivity. Time-dependent changes in the distribution $\eta(V)$ may characterize the rapidity of the cell response to variations in ambient conditions.

8. Conclusion

This paper expounds the dialogue problem as viewed by the author, educated as a physicist and having no systematic knowledge in biology. The solution to this interdisciplinary problem would permit better understanding the mechanism of self-organization of the cell's 'symphonic' orchestra and obtain a deeper insight into the origin of life. Despite the enormous complexity and multifacetedness of the questions touched upon in the paper, the results of medico–biological applications of coherent phase microscopy and progress in the development of new techniques [11, 12, 19–23] during the last 10 years give hope of fundamental discoveries in cell biophysics, molecular medicine, hematology, immunology, and pharmacology in the near future.

Besides its theoretical significance, the method also has important practical implications for cell biophysics, neurobiology [58], and molecular medicine. Indeed, the rationale of the method for measuring the metabolic component of refractivity and the introduction of the parameters χ_3 and $\delta n_{\max} = \langle \Delta n \rangle_{\max} - \langle \Delta n \rangle_{\min}$ (or the vitality $\delta n / \delta n_{\max} = V$) are paramount for the quantitative characteristic of the cell functional state. Histograms in the $\eta(V)$ coordinates may be useful for the quantitative evaluation of the action of external factors, diagnosis of the functional state and nonuniform distribution, etc. Other problems include cell resistance to pharmaceutical products, tests of the individual sensitivity to foreign proteins, prediction of graft rejection, express diagnosis of cancer, and cell viability. Time-dependent changes in the $\eta(V)$ distribution may serve as indicators of the cell response rapidity to variations in ambient conditions.

The up-to-date methods have the following advantages: the possibility of real-time measurements, the representation of results as quantitative values, broad universality, and the noncritical role of mechanisms of metabolic processes.

As noted above, modern biophysical methods do not yet employ the achievements of optoelectronics in full measure. There is a huge unexploited reserve of new techniques for registering, imaging, and analyzing signals underlain by the modern component basis coupled to computer methods. Taken together, they provide a promising new possibility for the improvement of microscope characteristics [23].

9. Appendix

It is a common practice to describe the properties of a multicomponent optical medium in terms of the electronic susceptibility. The following formula holds for the mean refractive index χ_Σ and the dielectric constant under the assumption that only three components (bulk water molecules χ_1, dry substance χ_2, and the metabolic component χ_3) additively contribute to the integrated medium susceptibility n_Σ:

$$\varepsilon = (1 + \chi_\Sigma) = n_\Sigma^2 \,. \tag{1}$$

We note that it is more correct to use χ_3 than the difference $\delta n = \langle \Delta n_{\max} \rangle - \langle \Delta n_{\min} \rangle$ to characterize physical changes in the medium. For metabolic and deenergized states, formula (1) takes the respective forms

$$\varepsilon_{\max} = \left(n_1 + \langle \Delta n_{\max} \rangle\right)^2 = 1 + \chi_1 + \chi_2 + \chi_3$$

$$\varepsilon_{\min} = \left(n_1 + \langle \Delta n_{\min} \rangle\right)^2 = 1 + \chi_1 + \chi_2 \,, \tag{2}$$

where $n_1 = n_0 = 1.33$. Formulas for the metabolic and dry components are derived from (2):

$$\chi_3 = \left(2n_1 + \langle \Delta n_{\max} \rangle + \langle \Delta n_{\min} \rangle\right)\left(\langle \Delta n_{\max} \rangle - \langle \Delta n_{\min} \rangle\right) ,$$

$$\chi_2 \cong 2 \langle \Delta n_{\min} \rangle n_1 \,. \tag{3}$$

For mitochondria at $\langle \Delta n_{\min} \rangle \cong 0.02$, $\langle \Delta n_{\max} \rangle \cong 0.07$, and $n_1 = 1.33$, formula (3) gives $\chi_1 = 0.77$, $\chi_2 = 0.053$, and $\chi_3 = 0.137$.

Thus, relative contributions to the polarization from the dry and metabolic components may have paradoxical values $\chi_2/\chi_1 \cong 7\%$ and $\chi_3/\chi_1 \cong 18\%$. The paradox consists in a considerable excess of the metabolic component over the dry one. Indeed, rapid inhibition of metabolism leads to a change in medium energization, whereas the chemical composition of the medium determining the dry component remains unaltered.

It is worth emphasizing the possibility of measuring the membrane charge density of an energized mitochondrion. At the characteristic value of the membrane potential $\Delta\Psi \cong 100$ mV and specific membrane capacity 1 μF cm^{-2}, the membrane charge density is described by the formula $q = \Delta\Psi C_0$. This implies the value $q \cong 10^{-7}$ Kl cm^{-2} or the surface density amounting to 10^4 elementary charges per 1 μm^{-2}, corresponding to the difference between charges at the inner membrane surface (ca. 10 nm). In this case, with the radius of the ion hydrate membrane being 2–3 nm, the fraction of bound water does not exceed 10%.

To measure the minimum amplitude of the signal δh that can be recorded in the correlation volume ΔV with a

fluctuation amplitude δn, it is assumed to be restricted by the noise of the device $\langle \Delta h \rangle$ and its spatial resolution. The area S of an actually resolvable element in the phase image is taken as a resolution characteristic. It may be smaller than the area of the Airy disk but must be larger than the area S of a single pixel. Then the amplitude resulting from a perturbation averaged over the surface element in the image can be found under the condition that $\delta h = \Delta V \delta n / S \geqslant \langle \Delta h \rangle$. The feasibility of this condition is illustrated by a numerical example. Measurements of a nucleolus signal with the sensitivity $\langle \Delta h \rangle = 1$ nm give $S = 0.03$ μm^2; hence, $\Delta V \delta n > 3 \times 10^{-5}$ μm^3. With the refractivity amplitude $\delta n = 0.03$, the minimal volume of spatially correlated fluctuations is $\Delta V = 10^{-3}$ μm^3, corresponding to the correlation radius about 0.1 μm. The formula

$$\chi_3 \cong 2n_1 \big(\langle \Delta n_{\max} \rangle - \langle \Delta n_{\min} \rangle \big) = 2n_1 \delta n$$

yields a rather large ($\delta \chi_3 \cong 8$ %) amplitude of the metabolic component of susceptibility.

Acknowledgements. The results reported in this paper were obtained at the Laboratory of Coherent Optics, MIREA, in 1995 – 2006. The author considers it his pleasant duty to express thanks to the laboratory staff and name the principal participants in the work. I V Mazalov, D V Ublinsky, and S I Klushin developed the microscope. A V Tavrov, G E Kufal', E V Perevedentseva, and T V Vyshenskaya performed the first measurements of biological objects. A V Kretushev made the most important contribution to the measurements and their analysis, and to software development over the last few years. For many years, T V Vyshenskaya prepared biological objects, measured them, and interpreted the results. I V Klemyashev, E N Slavnova, V V Lisovsky, and A B Ivanov participated in systematic cell measurements. Joint publications were prepared in the course of fruitful discussions and cooperation with A A Stil', A N Tikhonov, L S Yaguzhinsky, O V Zatsepina, I V Vasilenko, G I El'Registan, G V Maksimov, I V Reshetov, and D G Weiss. The work was supported by the RFBR Grant No. 07-04-00473.

References

1. Rapp P E *J. Exp. Biology* **81** 281 (1979)
2. Wang Y et al. *J. Cell Biol.* **174** 481 (2006)
3. Skulachev V P *Bioenergetika. Membrannye Preobrazovateli Energii* (Bioenergetics) (Biokhimiya Membran (Biochemistry of Membranes, Book 6, Ed. A A Boldyrev) (Moscow: Vysshaya Shkola, 1989)
4. Hüser J, Blatter L A *Biochem. J.* **343** 311 (1999)
5. Hattori T et al. *Biophys. J.* **88** 2340 (2005)
6. Brehm-Stecher B F, Johnson E A *Microbiol. Mol. Biol. Rev.* **68** 538 (2004)
7. Chentsov Yu S *Vvedenie v Kletochnuyu Biologiyu* (Introduction to Cell Biology) 4th ed. (Moscow: Akademkniga, 2004)
8. Naito Y, Toh-e A, Hamaguchi H *J. Raman Spectrosc.* **36** 837 (2005)
9. Huang Y-S et al. *J. Raman Spectrosc.* **35** 525 (2004)
10. Cheng J-X et al. *Biophys. J.* **83** 502 (2002)
11. Tychinskiĭ V P *Usp. Fiz. Nauk* **171** 649 (2001) [*Phys. Usp.* **44** 617 (2001)]
12. Tychinskiĭ V P et al. *Kvantovaya Elektron.* **24** 754 (1997) [*Quantum Electron.* **27** 735 (1997)]
13. Carl D et al. *Appl. Opt.* **43** 6536 (2004)
14. Lazebnik M et al. *Opt. Lett.* **28** 1218 (2003)
15. Vishnyakov G et al. *Microsc. Analysis* **18** (1) 19 (2004)
16. Langoju R, Patil A, Rastogi P *Opt. Express* **13** 7160 (2005)
17. Kleinfeld, Laporta A, in *Light Scattering Imaging of Neural Tissue Function* (Eds D M Rector, J S George) (Totowa, NJ: Humana Press, 2006)
18. Millerd J E et al. *Proc. SPIE* **5531** 304 (2004)
19. Rappaz B et al. *Opt. Express* **13** 9361 (2005)
20. Popescu G et al. *J. Biomed. Opt.* **10** 060503 (2005)
21. Ikeda T et al. *Opt. Lett.* **30** 1165 (2005)
22. Lue N et al. *Opt. Lett.* **31** 2759 (2006)
23. Park Y et al. *Opt. Express* **14** 8263 (2006)
24. Tychinsky V, Kretushev A, Vyshenskaja T *Eur. Biophys. J.* **33** 700 (2004)
25. Tychinsky V P et al. *Biochim. Biophys. Acta (BBA) — Biomembranes* **1665** 57 (2004)
26. Tychinsky V P et al. *Biochim. Biophys. Acta (BBA) — Bioenergetics* **1708** 362 (2005)
27. Tychinsky V P et al. *Biofizika* **45** 870 (2000) [*Biophysics* **45** 844 (2000)]
28. Tychinsky V P et al. *Dokl. Ross. Akad. Nauk* **405** 550 (2005) [*Dokl. Biochem. Biophys.* **405** 432 (2005)]
29. Tychinskii V P et al. *Byull. Eksp. Biol. Med.* **142** 465 (2006) [*Bull. Exp. Biol. Med.* **142** 481 (2006)]
30. Chissov V I et al. *Ross. Onkol. Zh.* (2) 11 (2006)
31. Tychinsky V P et al., in *Technical Proc. of the 2006 NSTI Nanotechnology Conf. and Trade Show* Vol. 2 (2006) (CDROM) Ch. 1
32. Kretushev A V, Tychinskii V P *Kvantovaya Elektron.* **32** (1) 66 (2002) [*Quantum Electron.* **32** 66 (2002)]
33. Tychinsky V P *Opt. Commun.* **74** 41 (1989)
34. Tychinskyii V P et al. *Pis'ma Zh. Eksp. Teor. Fiz.* **17** (22) 80 (1991) [*JETF Lett.* **17** 815 (1991)]
35. Microbiology by Lim, 2nd Edition, http://www.mhhe.com/biosci/cellmicro/limmicro/
36. Derenzini M et al. *J. Histochem. Cytochem.* **54** 131 (2006)
37. Dundr M, Misteli T *Biochem. J.* **356** 297 (2001)
38. Cheutin T et al. *J. Cell. Science* **115** 3297 (2002)
39. Raška I, Shaw P J, Cmarko D *Current Opin. Cell Biol.* **18** 325 (2006)
40. Lam Y W, Trinkle-Mulcahy L, Lamond A I *J. Cell. Science* **118** 1335 (2005)
41. White R J *Nature Rev. Mol. Cell Biol.* **6** 69 (2005)
42. Mayer C, Bierhoff H, Grummt I *Genes Dev.* **19** 933 (2005)
43. Dundr M et al. *Science* **298** 1623 (2002)
44. Grummt I *Genes Dev.* **17** 1691 (2003)
45. Jackson D A, Pombo A, Iborra F *FASEB J.* **14** 242 (2000)
46. Shevkunov S V *Khim. Vys. Energ.* **39** (6) (2005) [*High Energy Chem.* **39** (6) 351 (2005)]
47. Tychinsky V P et al. *Biol. Membrany* **22** (2) 13 (2005)
48. Gurau M C et al. *ChemPhysChem* **4** 1231 (2003)
49. Cheng J-X et al. *Proc. Natl. Acad. Sci. USA* **100** 9826 (2003)
50. Kim J, Kim G, Cremer P S *Langmuir* **17** 7255 (2001)
51. Wiggins P M *Cell Mol. Biol.* **47** 735 (2001)
52. Ling G, in *Interfacial Water in Cell Biology, Conf., South Hadley, MA, USA, June 6 – 11, 2004*
53. Pollack G H *Cells, Gels and the Engines of Life: a New, Unified Approach to Cell Function* (Seattle, WA: Ebner & Sons, 2001)
54. Chaplin M "Water structure and behavior", http://www.lsbu.ac.uk/water; "Nucleic acid hydration", http://www.lsbu.ac.uk/water/nucleic.html
55. Chen S-J, Dill K A *Proc. Natl. Acad. Sci. USA* **97** 646 (2000)
56. Li L, Mirny L A, Shakhnovich E I *Nature Struct. Biol.* **7** 336 (2000)
57. Pikin S A *Strukturnye Prevrashcheniya v Zhidkikh Kristallakh* (Structural Transformations in Liquid Crystals) (Moscow: Nauka, 1981) [Translated into English (New York: Gordon and Breach Sci. Publ., 1991)]
58. Maksimov GV et al. *Biofizika* **47** 345 (2002) [*Biophysics* **47** 330 (2002)]